Research article

Enhancing in-plane uniformity of graphene nanowalls using a rotating platform for solid-state lithium-ion battery

Rucheng Zhu[1,2,*], Yota Mabuchi[1], Riteshkumar Vishwakarma[1], Balaram Paudel Jaisi[1], Haibin Li[2], Masami Naito[1], Masayoshi Umeno[1] and Tetsuo Soga[2]

[1] C's Techno Inc., Coperative Research Center for Advanced Technology, Nagoya Science Park, Moriyama-ku, Nagoya Aichi 4630018, Japan
[2] Department of Electrical and Mechanical Engineering, Nagoya Institute of Technology, Gokiso-cho, Showa-ku, Nagoya, Aichi 466-8555, Japan

* Correspondence: Email: r.zhu.433@stn.nitech.ac.jp; Tel: +81-052-736-4382; Fax: +81-052-736-4382.

Abstract: In the realm of solid-state lithium-ion battery (SLIB) research, anode development remains a focal area because the interface between the solid electrolyte and the anode plays a critical role in determining battery performance. Among various anode materials, vertically aligned graphene nanowalls (GNWs) stand out as a promising candidate due to their extensive surface area, sharp exposed edges, and high conductivity. These features give GNWs great potential to enhance the efficiency and capacity of solid-state batteries. However, the plasma generated in microwave plasma chemical vapor deposition (MWPCVD) equipment chamber exhibits uneven distribution, making it challenging to achieve uniform growth of GNWs over a large area. To improve the in-plane uniformity during the growth of GNWs, a drive motor was installed beneath the substrate holder, allowing the substrate to rotate at a constant speed during the film deposition process, thus enhancing the in-plane uniformity of the GNWs. This paper also showed that the charge-discharge properties of SLIBs are improved with substrate rotation. Compared with the previously reported method of producing uniform microwave plasma through rapid rotation and slow pulsation in a resonant field, this modification of the apparatus is simpler. Additionally, the use of a mixed gas can effectively improve the uniformity of the in-plane GNW films, providing a viable reference for the mass production of SLIB anode electrodes.

Keywords: graphene; graphene nanowall; MWPCVD; solid-state lithium-ion battery; substrate rotation

1. Introduction

Over the years, humanity has developed and utilized a variety of energy sources and production technologies. In particular, in recent years, there has been a significant increase in research efforts toward new clean energy sources, effective energy conversion methods, and energy storage technologies, resulting in innovative advancements and breakthroughs in multiple fields of clean energy [1–3]. In the development of secondary batteries, lithium-ion batteries (LIBs) have gradually replaced lead-acid batteries, nickel-cadmium batteries, and nickel-metal hydride batteries as the mainstream in the market due to their high energy density, long cycle life, absence of memory effects, and low self-discharge rates [4–7]. Currently, liquid electrolytes dominate the battery technology landscape in LIBs because of their high ionic conductivity, broad temperature adaptability, design flexibility, and cost-effectiveness. However, liquid lithium-ion batteries also present challenges such as electrolyte leakage, poor thermal stability [8–11], environmental sensitivity, and poor cycle stability [12–14]. Consequently, the development of all-solid-state lithium-ion batteries, which use solid materials as electrolytes, has attracted the attention of researchers. In the development of anodes for solid-state lithium-ion batteries, silicon has been a main focus due to its exceptionally high specific capacity of 4800 mAh/g. However, the challenges of volume expansion and interface contact issues have been significant hurdles. Vertically aligned graphene nanowalls (GNWs) are emerging as a highly promising material due to their extensive surface area, sharp exposed edges, and high conductivity, which have the potential to address these challenges.

Current liquid electrolyte lithium-ion batteries predominantly employ graphite as the anode, benefiting from its low voltage, low cost, abundance, high energy density, power density, and extremely long cycle life. Consequently, in the research of all-solid-state lithium-ion batteries (SLIBs), graphite also becomes a primary subject of investigation. However, the theoretical specific capacity of graphite is only 372 mAh/g, and because the interface between the solid anode and the solid electrolyte only allows lithium-ion transport, the utilization of graphite is relatively lower compared with that of liquid electrolytes. Additionally, the formation of cracks at the solid–solid interface after multiple charge-discharge cycles impedes ion transport, significantly reducing the battery's cycle life [15–17]. For these reasons, exploring novel forms of carbon as anode materials has become a focal point of our research. GNWs decorated with silicon for the anode electrode of liquid lithium-ion batteries have been reported to achieve specific capacities that exceed 2000 mAh/g [18]. However, there are almost no papers on SLIB using bare GNWs.

Contrary to graphite, the carbon nanowalls consist of vertically standing nanosheets of graphene, hereby termed GNWs with high specific surface area. To obtain high-quality GNWs, we employed the microwave plasma chemical vapor deposition (MWPCVD) technique to deposit GNWs. This method allows the direct growth of GNWs on various substrates, including insulators, semiconductors, and metallic conductors [19–22]. However, because of the non-uniformity of the plasma during production, MWPCVD often results in insufficient in-plane uniformity of the films, which impacts the performance of SLIBs using GNWs as anodes, especially in terms of consistency in large-scale production [23–26]. There are reports that using a rapidly rotating resonant field and slow pulsation to produce a uniform microwave plasma can improve the uniformity in the plane of the deposited films and increase the film formation area [27–30]. However, this method requires significant modifications to the equipment and, to date, discharge test data using only a single gas are available. Whether the same effects can be achieved using mixed gases still requires further verification.

In this study, we innovatively adopted the method of using a rotating substrate holder, which allows for uniform film formation by adjusting the substrate's rotation without altering the current state of the plasma. This approach is simple in terms of modification, low in material costs, and easy to control operationally. Experiments have demonstrated that this method can achieve high in-plane uniformity during the large-scale preparation of GNWs films, and the morphological features of the GNWs are also significantly enhanced with substrate rotation. Moreover, we successfully produced a solid-state lithium-ion battery with an anode-specific capacity reaching up to 15.6 μAh/cm^2. This confirms that our method can effectively enhance the in-plane uniformity of GNWs while significantly improving their morphological features, facilitating better integration with the solid electrolyte. This research, with limited modifications to existing equipment, effectively improves the quality of GNWs and also reduces the manufacturing costs per unit. This paves the way for transitioning the development of GNW anodes for solid-state lithium-ion batteries from research and development to mass production.

2. Materials and methods

2.1. Equipment description

The MWPCVD equipment used in this study is illustrated in Figure 1 and consists of the following components:
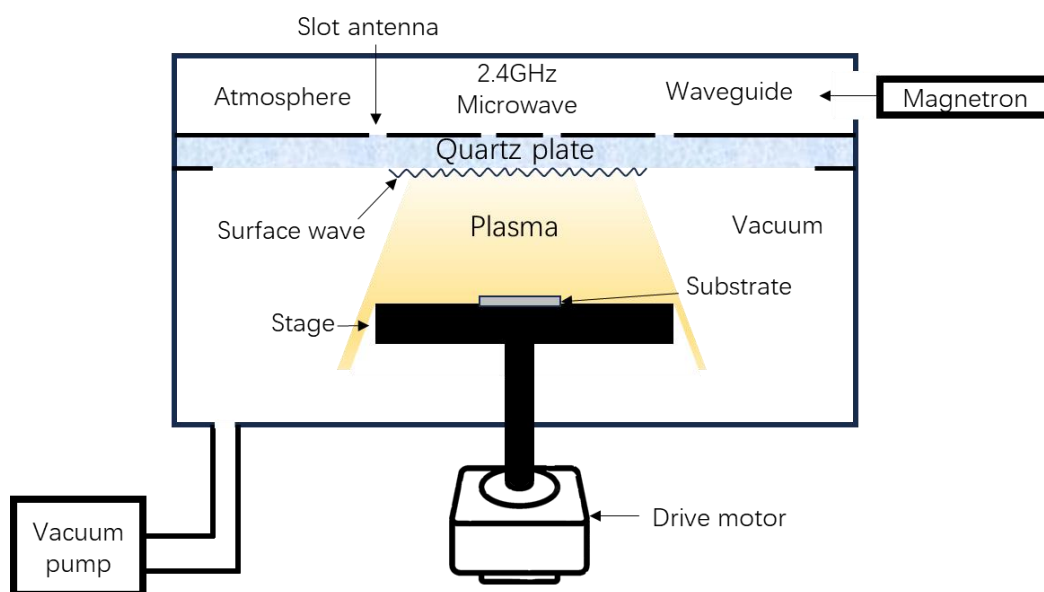

Figure 1. Schematic of the MWPCVD equipment.

Magnetron: generates 2.45 GHz microwave radiation.

Waveguide: guides the microwave radiation to the quartz plate.

Slot antenna: filters out unwanted harmonics and delivers the 2.45 GHz microwave radiation to the quartz plate.

Coupling adjustment knob: Adjusts the wave shape within the waveguide to ensure smooth transmission of microwaves through the slot antenna and into the quartz plate.

Quartz plate: allows microwave radiation to enter from its surface and undergoes total internal reflection inside, forming surface waves on the lower surface.

Gas inlet port: used to introduce precursor and carrier gases into the reaction chamber.

Rotatable stage: rotate with the sample.

Drive motor: drive the stage to rotate at a certain speed.

Vacuum pump: reduces impurities in the reaction chamber and maintains a low-pressure environment during the deposition process.

The equipment utilized in this study is an MWPCVD system collaboratively developed by C's Techno Inc., Chubu University, and Shinko Seiki Co.

2.2. Experimental conditions for GNWs

The GNW growth experiments were conducted under the following conditions: acetylene, hydrogen, and argon gases were used with flow rates of 5, 3, and 3 sccm, respectively, each with a purity of 99.999%. During the experiments, the substrate temperature was set at 500 °C, and the pressure in the reaction chamber was maintained at 8 Pa. The substrate material used was 304 stainless steel, and the growth duration was 10 min. This study involved two trials: in the first, the substrate holder remained stationary; in the second trial, the substrate holder rotated uniformly at a speed of 45 s per rotation. In these two trials, we prepared two GNW samples on 5 cm × 5 cm SUS substrates.

2.3. Fabrication and evaluation of solid-state lithium-ion battery

The solid-state electrolyte layer and the positive electrode layer were fabricated by radio frequency (RF) sputtering. A mixture of argon and nitrogen gases was employed as the sputtering gas at the anode. Li_3PO_3 was used as the target material for the electrolyte layer, with a 100W RF power source applied over a duration of 12 h for sputtering the electrolyte layer. Subsequently, $LiMn_2O_4$ was utilized as the cathode target material, with argon gas serving as the discharge gas. The cathode was sputtered using a 100 W RF power source for 6 h. Finally, a top layer consisting of a 1 cm^2 gold film was deposited to serve as the battery's current collector. The solid-state lithium-ion batteries were evaluated by cross-sectional scanning electron microscope (SEM) and charge-discharge properties.

3. Results and discussion

3.1. Optical and Raman spectroscopic analysis

Well after the GNWs growth, the chamber was cooled down to room temperature, and the GNW samples on the steel use stainless (SUS) substrate were photographed using a camera. A noticeable difference in color between the two specimens was observed.

Figure 2a,b represent the photographic images of the two samples of GNW that were grown without and with the stage rotation, respectively. From the two photographs, it is evident that there is a significant difference in the fiber optic reflection on the surfaces of the two samples. The GNWs on the sample from the stationary substrate holder caused light to scatter in various directions, resulting in a gradient color effect. In the sample from the rotating substrate holder, the reflected light did not exhibit noticeable diffraction or interference; therefore, the photograph displayed a uniform and

consistent color. Furthermore, we marked the two samples dividing them into nine regions each for further analysis of in-plane uniformity of GNWs' growth without and with the stage rotation as indicated in Figure 2.
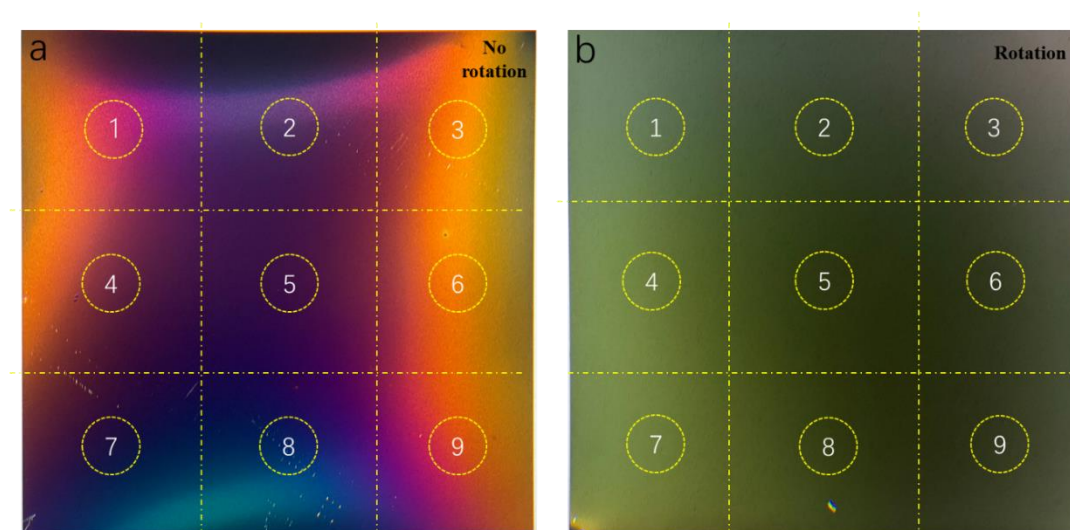

Figure 2. Photographic images of the samples: (a) without and (b) with rotation of the substrate holder rotation (sizes 5 cm × 5 cm).

Figure 3a,b show the Raman spectra around the nine different regions as indicated in Figure 2 without and with stage rotation, respectively. The presence of the graphitic (G), defect (D), and 2D peaks around 1590, 1345, and 2685 cm^{-1} confirms the growth of graphitic layers around all regions of the two samples. Furthermore, the existence of the hump peak (D^1) just right to the G peak around the wave number 1620 cm^{-1} signifies the growth of GNWs throughout the samples. Although there is no noticeable difference in the Raman spectra of the two samples, we further measured the peak heights of D, G, and 2D peaks of each spectrum of the two samples and plotted the D/G and 2D/G peak ratios. Figure 3c shows the D/G peak ratio of the two samples at the nine different regions. It is clear from Figure 3c that the reduced and almost constant D/G peak ratios around all nine regions of the rotating stage sample indicate the uniformity of GNWs' growth compared to the non-rotating stage sample. Analogous explanation fits for the comparatively uniform 2D/G peak ratios around the nine regions of the rotating stage sample in Figure 3d.
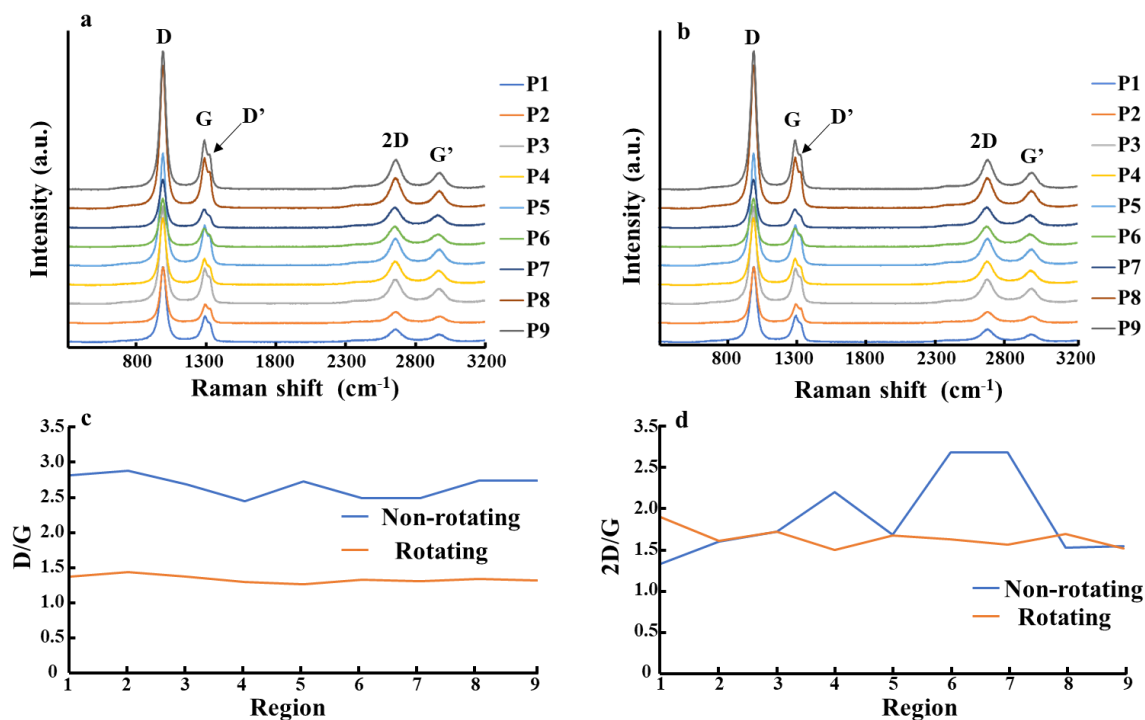
Figure 3. Raman spectra around the nine regions of the samples as indicated in Figure 2. (a) Without and (b) with stage rotations. Comparison of (c) the D/G peak ratio and (d) the 2D/G peak ratio of the two samples in different regions.

3.2. Observation of the morphology of GNWs using SEM

Figure 4 displays the magnified images of GNWs with a stationary substrate holder at different positions under the SEM. The images clearly show that the shapes of GNWs vary at each location. In particular, cross-sectional scans were performed at positions 1 and 8. The results indicate that the GNWs at position 1 are still in the early stages of growth with lower height and have not formed vertical walls; at position 8, while the specific shape of the GNWs has formed, the growth density is excessively high, which may impede the infiltration of the electrolyte.
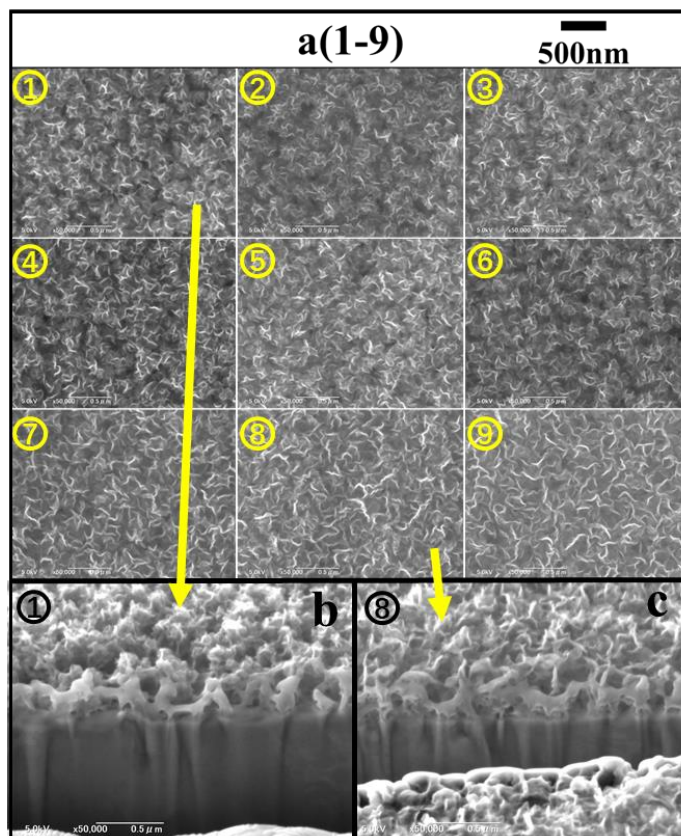
Figure 4. SEM images of the nine points from the GNWs sample with a stationary substrate holder, along with focused ion beam-scanning electron microscopy (FIB-SEM) cross-sectional images of points 1 and 8.

Figure 5 displays SEM images of GNWs prepared at various positions using a rotating substrate holder. In the nine positions shown in Figure 5, we can clearly observe the petal-shaped crystalline structures of the GNWs. To facilitate comparison with the GNW morphologies at the same positions (1 and 8) shown in Figure 5, cross-sectional scans were also conducted at positions 1 and 8. The cross-sectional images reveal the clear lamellar structure of the GNWs, with a uniform thickness of the flakes. This uniformity in flake thickness can enhance the contact area during the infusion of the solid electrolyte, potentially improving battery performance.
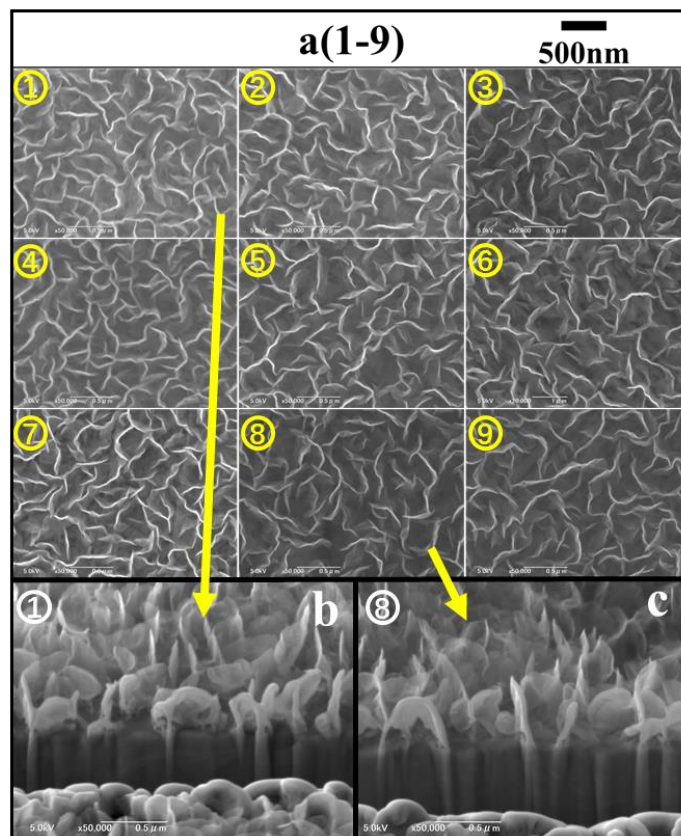
Figure 5. SEM images of the nine points from the GNWs sample with a rotating substrate holder, along with FIB-SEM cross-sectional images of points 1 and 8.

3.3. Discussion on instrumental modification for the in-plane uniformity of GNWs' growth

By comparing the FIB-SEM images from Figures 4 and 5, we observe that under the condition that the substrate holder does not rotate, there are significant variations in crystallization and height among the nine GNW sample points. On the contrary, with the rotation of the substrate holder, the changes in crystallinity and height are less pronounced, and the structure of the nanowalls can be clearly observed. On the non-rotating substrate holder, most sampling points show GNWs that are still in the initial stages of crystallization. This is primarily due to the uneven plasma density inside the MWPCVD chamber.
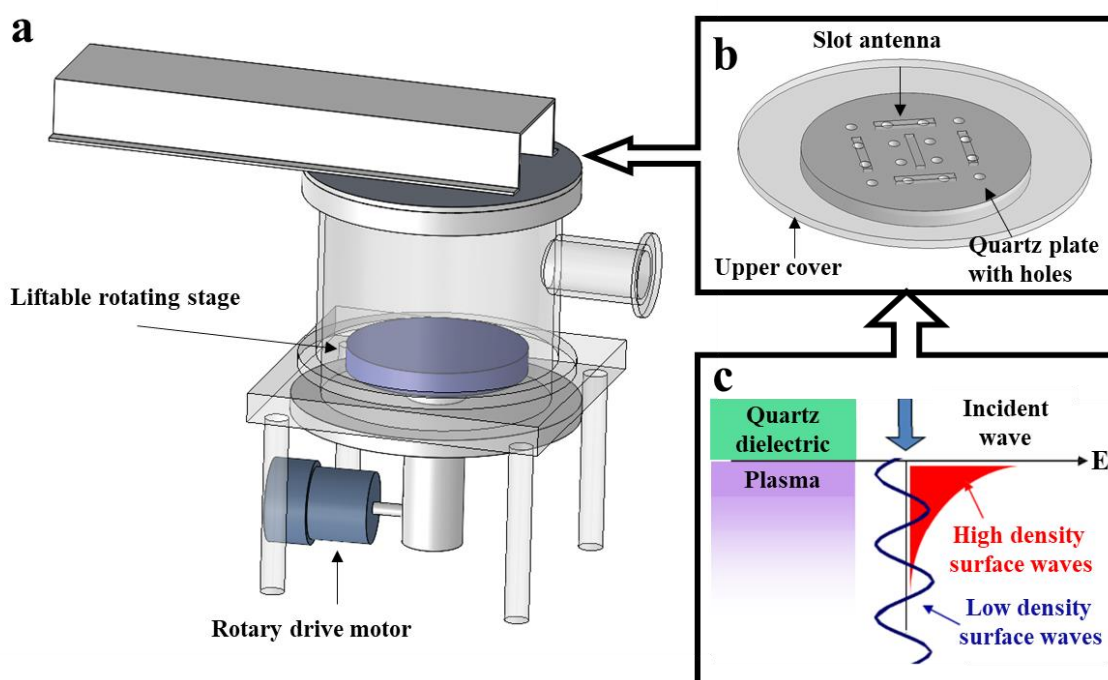
Figure 6. Schematic diagram of the MWPCVD apparatus.

As shown in Figure 6a, the MWPCVD system we used is a device that excites plasma using surface waves. The 2.45 GHz microwaves generated by a magnetron are directed onto the top cover of the apparatus via a waveguide. The microwaves enter the chamber through a slot antenna located in the top cover and impinge on a quartz plate beneath it, as illustrated in Figure 6b. Inside the quartz plate, the microwaves undergo total internal reflection and form surface waves that propagate along the outside of the plate. These surface waves spread across the quartz plate as shown in Figure 6c. The density of surface wave propagation decreases as the distance from the center of the incident wave increases. This phenomenon can be described by Eq 1 [31]:

$$d = \left(\frac{\omega}{c}\right)^2 \frac{\varepsilon_d(\omega_p{}^2 - \omega^2)}{\omega_p{}^2 - c(1+\varepsilon_d)\omega^2} - \left(\frac{\omega}{c}\right)^2 \left(1 - \frac{\omega_p{}^2}{\omega^2}\right) \tag{1}$$

In Eq 1, d represents the distance from the center of the incident wave, ω is the angular frequency of the incident wave, where $\omega = 2/\pi f$, and f is 2.45 GHz. c is the speed of light, ε_d is the dielectric constant of the medium, which in this case is the dielectric constant of quartz, and ε_p is the dielectric constant of plasma.

When electromagnetic waves irradiate gas atoms and molecules in the absence of a magnetic field, they excite them, forming a plasma composed of electrons and ions. This type of plasma wave, which propagates along the surface, can be excited by applying intense electromagnetic waves, creating a large diameter and high-density plasma. This phenomenon is known as surface wave plasma (SWP). In an environment of very thin air or vacuum, the energy from external electromagnetic waves accelerates the electrons in the atoms or molecules, generating plasma. When the frequency of the plasma's electrons matches the frequency of the microwaves, electromagnetic wave resonance absorption occurs, resulting in the formation of a high-density plasma. In this high-density plasma,

collisions between molecules and atoms lead to energy transfers, prompting neutral molecules and atoms to ionize into ions and electrons, exciting more molecules and atoms, and generating free radicals, achieving various active states. These active particles form the desired thin films on the substrate through diffusion.

However, as the energy of surface waves attenuates with distance, the density of the plasma also decreases, leading to spatially non-uniform distribution, which is a primary cause of poor in-plane uniformity in film formation. Yuichi Hasegawa and colleagues proposed that the generation of rotating plasma by increasing the injection of radial microwaves through radial antennas within a cylindrical cavity could positively affect the uniformity of the plasma within the chamber [30,31]. However, this method requires complex modifications to the equipment and has been tested only in an environment of a single gas; its effectiveness with mixed gases has not yet been assessed. We used a mixture of methane (or acetylene), hydrogen, and argon gases to generate carbon active particles, which, due to different ionization energies required, further exacerbate the non-uniform distribution of plasma within the chamber. This is another reason for the poor uniformity in the plane of the samples when not rotating. When the sample substrate is rotated within the plasma with the special modification on the liftable substrate holder using a rotating motor as shown in Figure 6a, as each position on the substrate periodically sweeps through plasma at the same height, the in-plane uniformity of GNWs on the sample can be significantly improved after a long deposition time.

3.4. Properties of a solid-state lithium-ion battery

In order to test the impact of sample uniformity on the battery, we used a fixture to make two 4-cell battery samples as shown in Figure 7a and conducted 10-cycle battery performance tests on each sample. After the charge and discharge cycle was completed, the sample at position 2 of the two samples was taken for FIB-SEM scanning, as shown in Figure 7b,c. During the cycle test, charging was performed using a constant current of 20 μA up to 4.2 V for a maximum of 5 h and discharging at 20 μA down to 0.5 V. As depicted in Figures 7d,e, all samples completed 10 cycles, except for sample d-3, which failed to achieve any charge-discharge cycles. During these cycles, the highest battery capacity was obtained on the first charge-discharge cycle, and the capacity gradually decreased with an increasing number of cycles. In Figure 7d (1–4), sample performance varied: sample 1 charged and discharged normally with a maximum capacity of 5 μAh/cm^2, while sample d-2 only reached 3.5 V; sample d-3 failed to cycle, and sample d-4 cycled but only reached 3.8 V and exhibited unstable voltage. In Figure 7e (1–4), all samples under the same cycling conditions completed cycles with capacities between 11 and 15.6 μAh/cm^2, indicating that GNWs grown on rotating substrates were more uniform, yielding better battery consistency.

Further analysis involved cross-sectional FIB-SEM scanning of sample 1 of both substrates; Figure 7b (this is a FIB-SEM cross-sectional scan of the sample shown in Figure 7d-1) shows that the tilt of the GNWs caused large spaces during electrolyte injection, inhibiting lithium-ion movement, and reducing battery performance. The failure of sample d-3 to cycle was largely due to insufficient electrolytes caused by voids leading to a short circuit. In contrast, Figure 7c (this is a FIB-SEM cross-sectional scan of the sample shown in Figure 7e-1) shows GNWs growing perpendicularly on the substrate, allowing full integration with the electrolyte and forming a large contact area, thus enhancing battery performance.
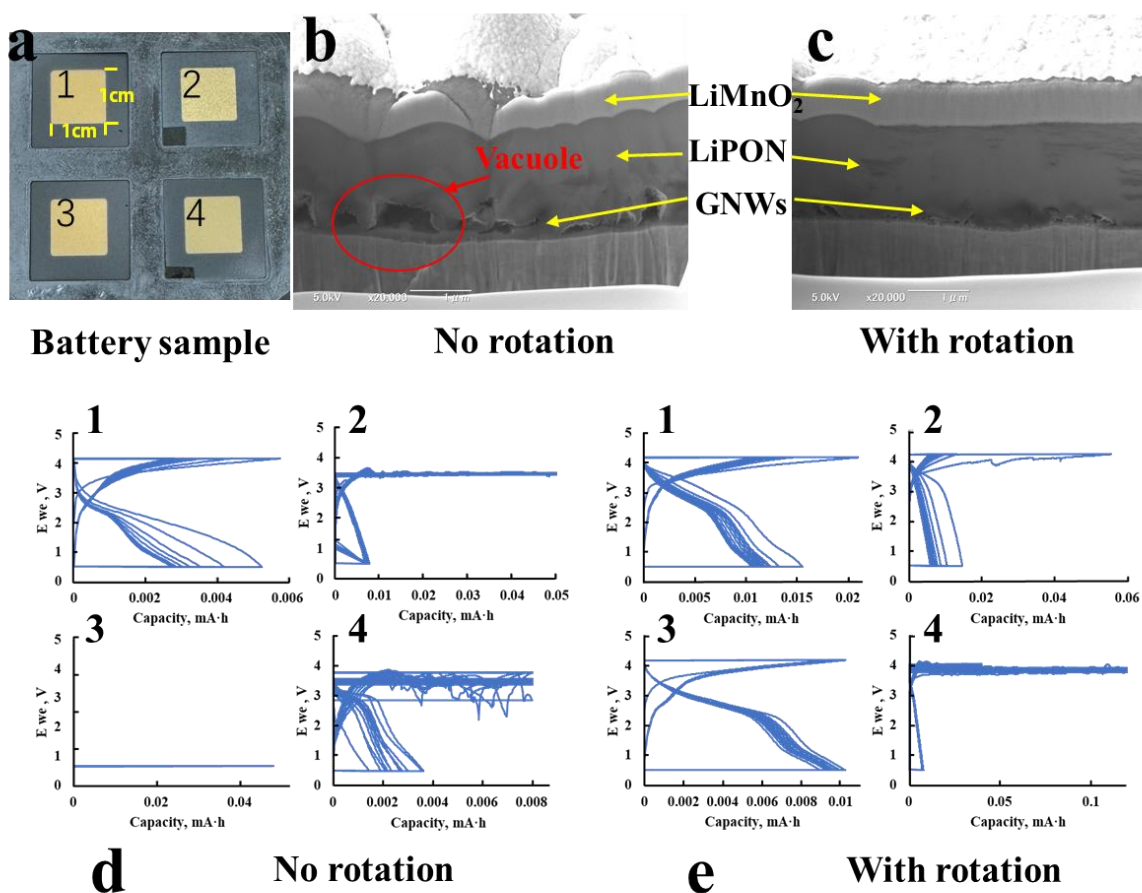
Figure 7. Construction and performance test of an all-solid-state lithium-ion battery with (a) photographic image of four cells under performance test, cross-sectional SEM images to show the construction of the device; (b) stationary substrate holder; and (c) rotating substrate holder. (d, e) Capacity test results of the four cells of each case.

4. Conclusions

We have successfully achieved uniform growth of GNW films on 5×5 cm SUS substrates and constructed prototypes of solid-state lithium-ion batteries with and without rotating substrate supports. We also tested the charge-discharge characteristics of batteries at four different positions on the 5×5 cm SUS substrates. Our method demonstrates that by simply altering the substrate support structure without modifying the microwave source or chamber structure, the quality and uniformity of the MWPCVD film deposition can be improved. The rotating GNW samples used had an average density of approximately $28\ \mu g/cm^2$, resulting in anode-specific capacities of up to $15.6\ \mu Ah/cm^2$ (555 mAh/g), which is approximately 1.5 times the capacity of graphite anodes. This technology reduces manufacturing costs per unit, enhances consistency in lithium-ion battery products, and provides a theoretical and technical foundation for the mass production of future all-solid-state lithium-ion batteries.

Use of AI tools declaration

The authors declare they have not used Artificial Intelligence (AI) tools in the creation of this article.

Acknowledgments

Author contributions

Rucheng Zhu: conceptualization, methodology, formal analysis, data curation, and original draft preparation; Yota Mabuchi: conceptualization, methodology; Riteshkumar Vishwakarma: resources, formal analysis; Balaram Paudel Jaisi: formal analysis, data curation, visualization and validation; Haibin Li: formal analysis, data curation, reviewing, and editing; Masami Naito: formal analysis, data curation, reviewing, and editing; Masayoshi Umeno: conceptualization, methodology, formal analysis, data curation, visualization, reviewing, and editing; Tetsuo Soga: conceptualization, methodology, formal analysis, data curation, visualization, reviewing, and editing.

Conflict of interest

Tetsuo Soga is editorial board member for *AIMS Materials Science* and was not involved in the editorial review or the decision to publish this article. The authors declare no conflict of interest.

References

1. Sikiru S, Oladosu TL, Amosa TI, et al. (2024) Hydrogen-powered horizons: Transformative technologies in clean energy generation, distribution, and storage for sustainable innovation. *Int J Hydrogen Energy* 56: 1152–1182. https://doi.org/10.1016/j.ijhydene.2023.12.186

2. Luan C, Sun X, Wang Y (2021) Driving forces of solar energy technology innovation and evolution. *J Clean Prod* 287: 125019. https://doi.org/10.1016/j.jclepro.2020.125019

3. Jain H (2024) From pollution to progress: Groundbreaking advances in clean technology unveiled. *Innovat Green Dev* 3: 100143. https://doi.org/10.1016/j.igd.2024.100143

4. Lopes P, Stamenkovic R (2020) Past, present, and future of lead–acid batteries. *Science* 369: 923–924. https://doi.org/10.1126/science.abd3352

5. Putois F (1995) Market for nickel-cadmium batteries. *J Power Sources* 57: 67–70. https://doi.org/10.1016/0378-7753(95)02243-0

6. Notten P, Ouwerkerk M, Van H, et al. (2004) High energy density strategies: from hydride-forming materials research to battery integration. *J Power Sources* 129: 45–54. https://doi.org/10.1016/j.jpowsour.2003.11.019

7. Choi J, Aurbach D (2016) Promise and reality of post-lithium-ion batteries with high energy densities. *Nat Rev Mater* 1: 1–16. https://doi.org/10.1038/natrevmats.2016.13

8. Blomgren G (2003) Liquid electrolytes for lithium and lithium-ion batteries. *J Power Sources* 119: 326–329. https://doi.org/10.1016/S0378-7753(03)00147-2

9. Hubble D, Brown D, Zhao Y, et al. (2022) Liquid electrolyte development for low-temperature lithium-ion batteries. *Energy Environ Sci* 15: 550–578. https://doi.org/10.1039/D1EE01789F

10. Yim T, Kwon M, Mun J, et al. (2015) Room temperature ionic liquid-based electrolytes as an alternative to carbonate-based electrolytes. *Israel J Chem* 55: 586–598. https://doi.org/10.1002/ijch.201400181

11. Tang X, Lv S, Jiang K, et al. (2022) Recent development of ionic liquid-based electrolytes in lithium-ion batteries. *J Power Sources* 542: 231792. https://doi.org/10.1016/j.jpowsour.2022.231792

12. Arbizzani C, Gabrielli G, Mastragostino M (2011) Thermal stability and flammability of electrolytes for lithium-ion batteries. *J Power Sources* 196: 4801–4805. https://doi.org/10.1016/j.jpowsour.2011.01.068

13. Zhang Q, Zhang X, Yuan H, et al. (2021) Thermally stable and nonflammable electrolytes for lithium metal batteries: Progress and perspectives. *Small Sci* 1: 2100058. https://doi.org/10.1002/smsc.202100058

14. Manthiram A (2017) An outlook on lithium ion battery technology. *ACS Cent Sci* 3: 1063–1069. https://doi.org/10.1021/acscentsci.7b00288

15. Cabañero M, Hagen M, Quiroga-González E (2021) In-operando Raman study of lithium plating on graphite electrodes of lithium ion batteries. *Electrochim Acta* 374: 137487. https://doi.org/10.1016/j.electacta.2020.137487

16. Zhang H, Yang Y, Ren D, et al. (2021) Graphite as anode materials: Fundamental mechanism, recent progress, and advances. *Energy Storage Mater* 36: 147–170. https://doi.org/10.1016/j.ensm.2020.12.027

17. Höltschi L, Jud F, Borca C, et al. (2020) Study of graphite cycling in sulfide solid electrolytes. *J Electrochem Soc* 167: 110558. https://doi.org/10.1149/1945-7111/aba36f

18. Krivchenko V, Itkis D, Evlashin S, et al. (2012) Carbon nanowalls decorated with silicon for lithium-ion batteries. *Carbon* 50: 1438–1442. https://doi.org/10.1016/j.carbon.2011.10.042

19. Davami K, Shaygan M, Kheirabi N, et al. (2014) Synthesis and characterization of carbon nanowalls on different substrates by radio frequency plasma enhanced chemical vapor deposition. *Carbon* 72: 372–380. https://doi.org/10.1016/j.carbon.2014.02.025

20. Hosu I, Sobaszek, Ficek M, et al. (2017) Carbon nanowalls: A new versatile graphene based interface for the laser desorption/ionization-mass spectrometry detection of small compounds in real samples. *Nanoscale* 9: 9701–9715. https://doi.org/10.1039/C7NR01069A

21. Bita B, Vizireanu S, Stoica D, et al. (2020) On the structural, morphological, and electrical properties of carbon nanowalls obtained by plasma-enhanced chemical vapor deposition. *J Nanomater* 1: 8814459. https://doi.org/10.1155/2020/8814459

22. Vishwakarma R, Zhu R, Abuelwafa A, et al. (2019) Direct synthesis of large-area graphene on insulating substrates at low temperature using microwave plasma CVD. *ACS Omega* 4: 11263–11270. https://doi.org/10.1021/acsomega.9b00988

23. Cho H, Kondo H, Ishikawa K, et al. (2014) Density control of carbon nanowalls grown by CH_4/H_2 plasma and their electrical properties. *Carbon* 68: 380–388. https://doi.org/10.1016/j.carbon.2013.11.014

24. Sugai H, Ghanashev I, Nagatsu M (1998) High-density flat plasma production based on surface waves. *Plasma Sources Sci Technol* 7: 192. https://doi.org/10.1088/0963-0252/7/2/014

25. Hotta M, Hasegawa Y, Nakamura K, et al. (2017) Generation of slowly rotating microwave plasma by amplitude-modulated resonant cavity. *Jpn J Appl Phys* 56: 116002. https://doi.org/10.7567/JJAP.56.116002

26. Asmussen J, Mallavarpu R, Hamann J, et al. (1974) The design of a microwave plasma cavity. *Proc IEEE* 62: 109–117. https://doi.org/10.1109/PROC.1974.9391

27. Kokura H, Yoneda S, Nakamura K, et al. (1999) Diagnostic of surface wave plasma for oxide etching in comparison with inductive RF plasma. *Jpn J Appl Phys* 38: 5256. https://doi.org/10.1143/JJAP.38.5256

28. Yeom H, Yoon M, Chae G, et al. (2023) Real-time monitoring of the plasma density distribution in low-pressure plasmas using a flat-cutoff array sensor. *Appl Phys Lett* 122: 114103. https://doi.org/10.1063/5.0129790

29. Ganachev I, Sugai H (2002) Production and control of planar microwave plasmas for materials processing. *Plasma Sources Sci Technol* 11: A178. https://doi.org/10.1088/0963-0252/11/3A/327

30. Yoshida Y, Ogura H (2000) Holey-plate plasma source for plasma processing. *Vacuum* 59: 459–465. https://doi.org/10.1016/S0042-207X(00)00302-X

31. Hasegawa Y, Nakamura K, Lubomirsky D, et al. (2017) Microwave plasma generation by the fast rotation and slow pulsation of resonant fields in a cylindrical cavity. *Jpn J Appl Phys* 56: 046203. https://doi.org/10.7567/JJAP.56.046203